Wangbai Pan
Department of Aeronautics and Astronautics,
Fudan University,
Shanghai 200433, China;
Department of Mechanical Engineering,
University of Connecticut,
Storrs, CT 06269
e-mail: 14110290001@fudan.edu.cn

Guoan Tang
Professor
Department of Aeronautics and Astronautics,
Fudan University,
Shanghai 200433, China
e-mail: tangguoan@fudan.edu.cn

Jiong Tang[1]
Professor
Department of Mechanical Engineering,
University of Connecticut,
Storrs, CT 06269
e-mail: jiong.tang@uconn.edu

Frequency Response-Based Uncertainty Analysis of Vibration System Utilizing Multiple Response Gaussian Process

This research concerns the uncertainty analysis and quantification of the vibration system utilizing the frequency response function (FRF) representation with statistical metamodeling. Different from previous statistical metamodels that are built for individual frequency points, in this research we take advantage of the inherent correlation of FRF values at different frequency points and resort to the multiple response Gaussian process (MRGP) approach. To enable the analysis, vector fitting method is adopted to represent an FRF using a reduced set of parameters with high accuracy. Owing to the efficiency and accuracy of the statistical metamodel with a small set of parameters, Bayesian inference can then be incorporated to realize model updating and uncertainty identification as new measurement/evidence is acquired. The MRGP metamodel developed under this new framework can be used effectively for two-way uncertainty propagation analysis, i.e., FRF prediction and uncertainty identification. Case studies are conducted for illustration and verification.
[DOI: 10.1115/1.4043609]

Keywords: frequency response function, vector fitting, multiple response Gaussian process, Bayesian inference, uncertainty quantification

1 Introduction

The characterization of dynamic properties of structures is the foundation for response analysis, system/fault identification, and control, where frequency response functions (FRFs) are commonly used to facilitate frequency-domain approaches. FRFs can be acquired from simulations of numerical models such as finite element models, or from testing/experiments on real structures. Critical dynamic information including resonant frequencies, damping ratios, and mode shapes can be further deduced from FRFs [1]. FRFs are generally sensitive to variations of structural properties and boundary conditions, which allows them widely used in optimal design [2], fault diagnosis [3,4], and control synthesis [5,6]. The existence of uncertainties in structures is inevitable due to tolerance in manufacturing, normal variations in material and geometry properties, and in-service degradation, etc. [7]. Uncertainty effects need to be considered in structural design, and also continuously monitored in service life. Uncertainty analysis and quantification focus on studying the cause and consequence of uncertain structural parameters. In the forward analysis, uncertainties are typically introduced through assigning prior probabilistic distributions of structural parameters. Monte Carlo simulation can then be conducted to capture the performance/response variation through sampling in the parametric space. FRFs are often used to reveal the uncertainty effects in the frequency domain. The variation of an FRF can be analyzed through Monte Carlo sampling with repeated simulations or experiments under uncertainty parameters.

It is, however, practically infeasible to carry out physical experiments with a large number of sampled uncertainty parameters. It is also computationally costly and even prohibitive to perform a repeated calculation of high-resolution FRFs through Monte Carlo sampling, especially for large-scale structures with high dimensionalities. There has been significant recent interest in developing methods that can efficiently characterize the variations in FRFs. One type of approaches is modal based. Muscolino et al. [8] used the modal analysis on the nominal model followed by perturbation analysis to predict FRF variation. Hinke et al. [9] carried out component mode synthesis based order reduction to improve the analysis efficiency, and FRF envelops under uncertainty effect were obtained through perturbation. Yang et al. [10] adopted polynomial chaos expansion method with order-reduced model to analyze the frequency response variations. In these studies, a nominal model was analyzed to obtain the baseline modal information, e.g., mode shapes and natural frequencies, and then uncertainty propagation computation was facilitated. It is worth noting that in many cases the complete modal information is difficult to acquire. Usually, a very limited number of measurement points can be realized in experimental modal analysis. It is very hard to obtain higher-order mode shapes accurately in both experimental and numerical analyses.

Another type of approach is built upon the idea of improving the efficiency of statistical sampling. For example, a small number of FRF results sampled from the given uncertainty parameters are obtained first. Then, a statistical metamodel is established based on these results, so that any FRF in the uncertain parametric space can be predicted directly from this metamodel without using the original numerical model or performing new experiments. This is similar to the supervised learning concept in machine learning. Gaussian process (GP) regression has been one class of popular algorithms adopted in dynamic analysis to derive the metamodels [11–13]. Xia and Tang [7] calculated the coarse FRF values at a small number of frequency points and then developed GP metamodel to estimate the high-resolution FRF, which reduced the computational cost for a single run. Fricker et al. [14] and Diazdelao et al. [15] both studied the prediction of FRFs under uncertainties by building independent GP models at each frequency point individually. Although efficient in characterizing the variation of an FRF at key frequency points, this kind of method become tedious when the variation of the entire FRF is of interest. A very large number of

[1]Corresponding author.

Contributed by the Technical Committee on Vibration and Sound of ASME for publication in the Journal of Vibration and Acoustics. Manuscript received April 16, 2018; final manuscript received April 18, 2019; published online June 5, 2019. Assoc. Editor: Maurizio Porfiri.

frequency points are needed in high-resolution FRF representation, and independent GP models will have to be established for all the frequency points. Essentially, GP models developed independently for different frequency points neglect the inherent correlation of FRF values at different frequency points.

Recently, methods of developing metamodels based on multiple response Gaussian process (MRGP) have attracted attention [16,17]. These methods give consideration to the correlation among multiple outputs. Arendt et al. [16] pointed out that the advantage of MRGP metamodel was that, when multiple responses are mutually dependent on the same set of parameters, the information obtained from them can be combined to better infer the true response values corresponding to these parameters. Intuitively, one may apply this MRGP framework to facilitate FRF variation prediction. As noted by Arendt et al. [16], however, MRGP can be employed only when the number of dependent response variables is small. The frequency points involved in high-resolution FRF is very large especially for structures that are lightly damped (in order to capture the peak responses). Therefore, in reality, the direct application of MRGP to high-resolution FRF is still computationally infeasible.

Meanwhile, a fundamental feature of statistical metamodels including those established based on GP or MRGP is that they all provide likelihood estimation of their prediction. This leads to an important, potential advantage to conduct the uncertainty quantification and identification, i.e., the inverse analysis, by incorporating the Bayesian inference framework. Bayesian inference is a statistical method in which the Bayes' rule is utilized to update the probability estimation with a hypothesis as additional evidence is obtained [18]. The hypothesis in our case refers to the prior probability of uncertainty parameters and the likelihood estimation derived from Gaussian process [19,20]. Bayesian inference thus is able to derive the posterior probability of uncertainty parameters. Maximum likelihood estimation or optimization processes can be carried out to determine the values with the greatest probability [13,21,22], which essentially leads to the quantification of uncertainty parameters. While the idea of integrating Bayesian inference into FRF-based uncertainty analysis is appealing since the measurement data of FRF can be obtained in a straightforward manner, the actual implementation has not been widely seen. One challenging issue here is how to parametrize the uncertainty parameters so the inverse identification is computationally tractable. Obviously, directly updating the original numerical model (e.g., the finite element model) without any prior empirical knowledge of uncertainties (e.g., type, location) may not be executable.

The objective of this research is to advance the state-of-the-art in FRF-based uncertainty analysis and quantification by addressing the aforementioned issues and challenges. Using a small number of FRFs obtained in the uncertain parametric space as sampled knowledge, we formulate an efficient MRGP-based approach to establish a statistical metamodel that yields the functional relation between uncertainty parameters and FRF results, which can facilitate variation analysis of FRF of structural systems with uncertainty. In the MRGP model establishment, uncertainty parameters are considered as the input. To make the MRGP formulation computationally tractable, we take advantage of the vector fitting method [23,24] to represent an FRF as a summation of rational fractions, which can parameterize effectively the FRF with a small number of parameters. These parameters are used as the output of the MRGP model. Once the MRGP model is built, the FRF under uncertainty parameters can be predicted directly without carrying out simulations or experiments. We further devise a Bayesian inference approach to realize uncertainty identification. That is, when a new FRF is acquired, it is used as new evidence to update the prior knowledge of uncertainty parameters, e.g., their probability distributions. The posterior knowledge can quantify which uncertainty parameters are most likely to generate the new given FRF. This two-way uncertainty propagation analysis, FRF prediction and uncertainty identification, is computationally efficient and accurate and takes full advantage of the correlation of the FRF values at different frequency points. The rest of this paper is organized as follows. Section 2 outlines the rational fraction expansion of FRF for linear systems as well as the FRF parameterization process. The details of establishing MRGP metamodel and the formulation of uncertainty quantification and identification by Bayesian inference are presented in Sec. 3. Section 4 illustrates the effectiveness and efficiency of the FRF-based uncertainty analysis and quantification through case investigations. Concluding remarks are given in Sec. 5.

2 Frequency Response Function of Vibration System and Its Vector Fitting

In this section, we present the formulation of the rational fraction expansion of FRF for linear vibration system, followed by a parametrization process for FRF. The parametrized FRF is the basis for the subsequent uncertainty analysis and quantification.

2.1 Frequency Response Function and Rational Fraction Expansion.

We consider a linear vibration system with n_f degrees-of-freedom (DOFs)

$$\mathbf{M}\ddot{\mathbf{x}} + \mathbf{C}\dot{\mathbf{x}} + \mathbf{K}\mathbf{x} = \mathbf{f} \tag{1}$$

where $\mathbf{M}$, $\mathbf{C}$, and $\mathbf{K}$ denote, respectively, the mass, damping, and stiffness matrices. Consider harmonic excitation $\mathbf{f}(t) = \mathbf{F}e^{i\omega t}$ where $\mathbf{F}$ is a constant vector of force magnitude and ω is the sweeping frequency. We have the vector-form FRF of the structure as

$$\mathbf{X} = \mathbf{T}(\omega)\mathbf{F} \tag{2}$$

where $\mathbf{T}(\omega) = (-\omega^2\mathbf{M} + i\omega\mathbf{C} + \mathbf{K})^{-1}$ is the transfer matrix of this system. Each vector component in $\mathbf{X}$ is the FRF at the corresponding DOF. The FRF can be obtained by directly calculating the transfer function at sweeping frequency points. This however generally leads to high computational cost, especially for high-resolution FRF with a large number of frequency points.

Alternatively, $\mathbf{X}$ can be expressed as the summation of rational fractions with modal information as

$$\mathbf{X} = \left(\sum_{k=1}^{2n_f} \frac{\boldsymbol{\varphi}_k \boldsymbol{\varphi}_k^T}{i\omega - \lambda_k}\right)\mathbf{F} \tag{3}$$

where λ_k and $\boldsymbol{\varphi}_k$ $(k = 1, 2, \ldots 2n_f)$ are the complex eigenvalues and eigenvectors of the following second-order eigenvalue problem

$$(\lambda_k^2\mathbf{M} + \lambda_k\mathbf{C} + \mathbf{K})\boldsymbol{\varphi}_k = \mathbf{0} \tag{4}$$

The above eigenvalue problem can be solved in the state space [25,26]. The eigenvectors satisfy the weighted orthogonality condition and normalization condition [27], i.e.,

$$\lambda_j\boldsymbol{\varphi}_j^T\mathbf{M}\boldsymbol{\varphi}_k + \lambda_k\boldsymbol{\varphi}_j^T\mathbf{M}\boldsymbol{\varphi}_k + \boldsymbol{\varphi}_j^T\mathbf{C}\boldsymbol{\varphi}_k = 0, \quad j \neq k \tag{5a}$$

$$2\lambda_k\boldsymbol{\varphi}_k^T\mathbf{M}\boldsymbol{\varphi}_k + \boldsymbol{\varphi}_k^T\mathbf{C}\boldsymbol{\varphi}_k = 1 \tag{5b}$$

For a classical vibration system where the damping matrix $\mathbf{C}$ is symmetric, both the eigenvalues and the eigenvectors exist in the form of conjugate pairs as $\lambda_k = \bar{\lambda}_{k+n_f}$ and $\boldsymbol{\varphi}_k = \bar{\boldsymbol{\varphi}}_{k+n_f}$ $(k = 1, \ldots, n_f)$. Equation (3) can be rewritten as

$$\mathbf{X} = \left[\sum_{k=1}^{n_f}\left(\frac{\mathbf{E}_k}{i\omega - \lambda_k} + \frac{\bar{\mathbf{E}}_k}{i\omega - \bar{\lambda}_k}\right)\right]\mathbf{F} \tag{6}$$

where $\mathbf{E}_k = \boldsymbol{\varphi}_k\boldsymbol{\varphi}_k^T$. Thus, each component X_i of $\mathbf{X}$, i.e., the FRF of each DOF, is expressed through rational fraction expansion as

$$X_i = \sum_{k=1}^{n_f}\left(\frac{\alpha_{ik}}{i\omega - \lambda_k} + \frac{\bar{\alpha}_{ik}}{i\omega - \bar{\lambda}_k}\right), \quad i = 1, \ldots, n_f \tag{7}$$

where α_{ik} is the ith component in vector $\mathbf{E}_k\mathbf{F}$. It can be readily observed that all X_i share the identical set of denominators (i.e., $i\omega - \lambda_k$ and $i\omega - \bar{\lambda}_k$) but have different numerators (i.e., α_{ik} and $\bar{\alpha}_{ik}$) in the summation expression. Apparently, when the FRF is to be analyzed at a large number of frequency points, the rational fraction expansion will be a more efficient option when compared with the matrix inversion approach (i.e., finding the transfer matrix $\mathbf{T}(\omega)$ directly at different frequency points), because the modal information only has to be extracted once, regardless of the number of frequency points involved.

2.2 Parametrization of Frequency Response Function Through Rational Approximation by Vector Fitting Method. In terms of FRF analysis, the expression given by Eq. (6) or Eq. (7) still has limitations. It is generally impractical to compute or experimentally extract the complete modal information (i.e., the complete sets of eigenvalues/natural frequencies and eigenvectors/modes). In computational analysis, besides the issue of high computational cost involved in extracting higher-order eigenvalues/eigenvectors, the results solved at very high frequencies may not be credible at all. In experimental analysis, usually modal information can only be extracted within a limited frequency range, and since the number of sensors is also limited the mode shape information is incomplete. Equation (7), on the other hand, indicates that practically not all the terms in the summation expression have to be kept. One should mainly focus on the terms with eigenvalues having absolute values $|\lambda_k|$ within or close to the frequency range of interest. This inspires us to utilize the vector fitting method [23] to develop a rational fraction expansion with a considerable smaller number of summation terms to express the FRF. The vector fitting method has been employed in the frequency-domain modeling of a variety of systems [28–30]. Here, we use this method to develop a numerically efficient expression for the FRF of interest.

Let us consider FRFs at n_c DOFs where n_c can be the number of sensors employed in the experiment. Under frequency-sweeping excitation, the FRFs at these DOFs are obtained simultaneously at discrete frequency points. The vector fitting method indicates that this set of FRFs can be fitted as [31]

$$X_i \approx \sum_{k=1}^{n_p/2}\left(\frac{\gamma_{ik}}{i\omega-\mu_k}+\frac{\bar{\gamma}_{ik}}{i\omega-\bar{\mu}_k}\right), \quad i=1,\ldots,n_c,\ \omega_L\le\omega\le\omega_R \tag{8}$$

where n_p, which must be an even number here, is the number of poles used for vector fitting, and ω_L and ω_R are the lower and upper bounds of the frequency range of concern. n_p may be selected empirically to fit specific accuracy requirement, and a practical choice is $n_p = 2n_0 + 4$, in which n_0 is the number of natural frequencies within the concerned frequency range. γ_{ik} and μ_k in Eq. (8) are coefficients derived based on the pole allocation process. To illustrate the pole allocation process, let us first consider the case where $n_c = 1$ and thus only 1DOF is involved in FRF measurement, resulting in the FRF X_1. We assume an unknown rational fraction function with random initial poles $\tilde{\mu}_k$ as

$$\theta(\omega)=\sum_{k=1}^{n_p}\left(\frac{\tilde{\gamma}_{1k}}{i\omega-\tilde{\mu}_k}\right)+1 \tag{9}$$

We then use the same poles to express the result of $\theta(\omega)X_1(\omega)$ as

$$\theta(\omega)X_1(\omega)=\sum_{k=1}^{n_p}\left(\frac{\hat{\gamma}_{1k}}{i\omega-\tilde{\mu}_k}\right)+\tilde{d} \tag{10}$$

where $\tilde{d}$ represents an unknown zero-order constant term. Combining Eqs. (9) and (10), we have

$$\left[\sum_{k=1}^{n_p}\left(\frac{\tilde{\gamma}_{1k}}{i\omega-\tilde{\mu}_k}\right)+1\right]X_1(\omega)=\sum_{k=1}^{n_p}\left(\frac{\hat{\gamma}_{1k}}{i\omega-\tilde{\mu}_k}\right)+\tilde{d} \tag{11}$$

or

$$\sum_{k=1}^{n_p}\left(\frac{\tilde{\gamma}_{1k}X_1(\omega)}{i\omega-\tilde{\mu}_k}\right)-\sum_{k=1}^{n_p}\left(\frac{\hat{\gamma}_{1k}}{i\omega-\tilde{\mu}_k}\right)-\tilde{d}=-X_1(\omega) \tag{12}$$

In Eqs. (9)–(12), $\tilde{\gamma}_{1k}$, $\hat{\gamma}_{1k}$, and $\tilde{d}$ are all unknown variables to be solved later. An FRF X_1 contains results from multiple discrete frequency points, and at each frequency point ω_i we have

$$\sum_{k=1}^{n_p}\left(\frac{\tilde{\gamma}_{1k}X_1(\omega_i)}{i\omega-\tilde{\mu}_k}\right)-\sum_{k=1}^{n_p}\left(\frac{\hat{\gamma}_{1k}}{i\omega-\tilde{\mu}_k}\right)-\tilde{d}=-X_1(\omega_i) \tag{13}$$

Clearly, Eq. (13) is linear with respect to all the unknown variables. These unknown variables can be solved via the least square method by combining the equations from all frequency points. We then have

$$X_1(\omega)=\frac{\sum_{k=1}^{n_p}\left(\frac{\hat{\gamma}_{1k}}{i\omega-\tilde{\mu}_k}\right)+\tilde{d}}{\sum_{k=1}^{n_p}\left(\frac{\tilde{\gamma}_{1k}}{i\omega-\tilde{\mu}_k}\right)+1}=\frac{\prod_{k=1}^{n_p}\frac{(i\omega-\hat{z}_{1k})}{(i\omega-\tilde{\mu}_k)}}{\prod_{k=1}^{n_p}\frac{(i\omega-\tilde{z}_{1k})}{(i\omega-\tilde{\mu}_k)}}=\prod_{k=1}^{n_p}\frac{(i\omega-\hat{z}_{1k})}{(i\omega-\tilde{z}_{1k})} \tag{14}$$

where $\tilde{z}_{1k}$ and $\hat{z}_{1k}$ are the zeros of $\theta(\omega)$ and $\theta(\omega)X_1(\omega)$, respectively. Equation (14) indicates that the zeros $\tilde{z}_{1k}$ solved from $\theta(\omega)$ are actually the poles of $X_1(\omega)$ after elimination. In practice, several iterations will be performed to repeat the process above (using newly solved poles to replace the current ones) to yield convergent poles μ_k and then to determine γ_{1k} by simplifying Eq. (14) into summation form. Owing to the nature of FRF, μ_k and γ_{1k} solved will also exist in the form of conjugate pairs, similar to that shown in Eq. (7).

The pole allocation processes for multiple FRFs $\{X_i\}(i=1,\ldots,n_c)$ are essentially similar, and all $X_i(\omega)$ will share the same poles as they come from the same underlying mechanical system. As will be shown later in the case study, when the number of poles is properly determined, the fitted FRF curves match the original data very well.

This fitting process itself only requires the FRF results obtained either numerically or experimentally, thereby avoiding the difficulty associated with obtaining the complete modal information for expansion. Both n_c and $n_p/2$ are much smaller than n_f, the number of DOFs of the original system. Fundamentally, the set of n_c FRFs is parameterized into $n_p \times (n_c + 1)$ real parameters, i.e.,

$$\{X_i\}(i=1,\ldots,n_c)\rightarrow\mathbf{y}=[\boldsymbol{\alpha}_1,\boldsymbol{\alpha}_2,\ldots,\boldsymbol{\alpha}_{n_p/2}] \tag{15}$$

where

$$\boldsymbol{\alpha}_k=[\text{real}(\mu_k),\text{imag}(\mu_k),\text{real}(\gamma_{1k}),\text{imag}(\gamma_{2k}),\ldots,\text{real}(\gamma_{n_ck}),\ \text{imag}(\gamma_{n_ck})],\quad k=1,\ldots,n_p/2 \tag{16}$$

In either computational analysis or experimental analysis, in order to capture important information such as resonant peaks, the frequency resolution has to be very high, leading to a very large number of frequency points involved. This vector fitting method can significantly reduce the parameters required to describe an FRF. Meanwhile, Eq. (8) for FRF after fitting is a C-infinity function, which helps to interpolate the FRF value at any other frequency point that is not included in the original FRF data.

3 Uncertainty Analysis and Quantification of Frequency Response Function

Here in this section, we discuss uncertainty analysis and quantification of the frequency response function. We start from the formulation of a statistical metamodel that can efficiently predict the variation of frequency response function parametrized through the vector fitting method. We then present a Bayesian inference approach to update the uncertainty parameter distribution and

predict the uncertainty parameters when new results/measurements are acquired.

3.1 Multiple Response Gaussian Process Modeling of Frequency Response Function. Gaussian process regression has seen increased usage in developing metamodels that can rapidly predict output under given input through emulation. In this research, we resort to a MRGP modeling approach to perform uncertainty analysis of FRFs. Here, instead of predicting variation of FRF at individual frequency point, we directly analyze the variation of the FRF as a function. That is, the metamodel output is the set of parameters employed to describe the corresponding FRF (Eq. (15)). Assume the original mechanical system contain n_u uncertainty parameters that are the input variables of the MRGP metamodel. Also assume FRFs are evaluated at n_c DOFs, and n_p poles are used in vector fitting to parametrize the FRFs, leading to an n_q ($n_q = n_p \times (n_c + 1)$) dimensional output (Eq. (15)). n_s sampled uncertainty inputs and their corresponding parameterized FRFs outputs are used to form the MRGP model. The prior for the MRGP model is [16,32,33]

$$\mathbf{y}(\mathbf{p}) \sim \mathrm{GP}[\mathbf{h}(\mathbf{p})\mathbf{B}, \boldsymbol{\Sigma}\mathbf{R}(\mathbf{p}, \mathbf{p}')] \tag{17}$$

where $\mathbf{p} = [p_1, p_2, \ldots, p_{n_u}]$ is the input row vector representing n_u uncertainty parameters, and $\mathbf{y}(\mathbf{p})$ denotes the multiple responses under given input, which in the FRF analysis case is a row vector shown in Eq. (15) as $\mathbf{y}(\mathbf{p}) = [\boldsymbol{\alpha}_1, \boldsymbol{\alpha}_2, \ldots, \boldsymbol{\alpha}_{n_p/2}] = [y_1, y_2, \ldots, y_{n_q}]$, i.e., the parameters of FRF after vector fitting.

The prior mean function comprises a row vector of specified regression functions $\mathbf{h}(\mathbf{p})$ and a matrix of unknown regression coefficients $\mathbf{B}$. In this research, we use $\mathbf{h}(\mathbf{p}) = [1, p_1, \ldots, p_{n_u}]$ to capture the linear characteristic under small uncertainties. Correspondingly, we define $\mathbf{B} = [\boldsymbol{\beta}_1, \ldots, \boldsymbol{\beta}_{n_q}]$, in which $\boldsymbol{\beta}_i = [\beta_{i,1}, \ldots, \beta_{i,1+n_u}]^T$ is the unknown regression coefficient vector for the ith element of output vector $\mathbf{y}(\mathbf{p})$. The prior covariance function is the product of an unknown nonspatial $n_q \times n_q$ covariance matrix $\boldsymbol{\Sigma}$ and a spatial $n_s \times n_s$ correlation matrix $\mathbf{R}$. Σ_{ij} in $\boldsymbol{\Sigma}$ represents the covariance between the ith and the jth outputs. R_{mn} in $\mathbf{R}$ represents the correlation between the mth and nth input sets of uncertainty parameters, determined by a Gaussian correlation function as

$$R_{mn} = R(\mathbf{p}_m, \mathbf{p}_n) = \exp\left\{-\sum_{k=1}^{n_u} \kappa_k (p_{m,k} - p_{n,k})^2\right\} \tag{18}$$

where $\boldsymbol{\kappa} = [\kappa_1, \ldots, \kappa_{n_u}]$ is the vector of roughness parameters that represent the correlation between two inputs/uncertainty parameters. Thus, the arbitrary covariance between any two output results can be written as

$$\mathrm{Cov}[y_i(\mathbf{p}_m), y_j(\mathbf{p}_n)] = \Sigma_{ij} R_{mn} \tag{19}$$

We now refer to $\phi = \{\mathbf{B}, \boldsymbol{\Sigma}, \boldsymbol{\kappa}\}$ as the hyperparameters of the MRGP metamodel. With given response data $\mathbf{Y} = [\mathbf{y}^T(\mathbf{p}_1), \ldots, \mathbf{y}^T(\mathbf{p}_{n_s})]^T$ under n_s sampled uncertainty sets $\mathbf{P} = [\mathbf{p}_1^T, \ldots, \mathbf{p}_{n_s}^T]^T$, these hyperparameters can be obtained from the maximum likelihood estimation [11,34]. The multivariate normal likelihood function is

$$p(\mathbf{Y}|\mathbf{B}, \boldsymbol{\Sigma}, \boldsymbol{\kappa}) = (2\pi)^{-n_q n_s/2} (\det \boldsymbol{\Sigma})^{-n_s/2} (\det \mathbf{R})^{-n_q/2} \exp\left\{-\frac{1}{2}\mathrm{vec}(\mathbf{Y} - \mathbf{HB})^T (\boldsymbol{\Sigma} \otimes \mathbf{R})^{-1} \mathrm{vec}(\mathbf{Y} - \mathbf{HB})\right\} \tag{20}$$

where vec() denotes the vectorization operator to stack the columns of a matrix in sequence to form a long column vector, $\otimes$ denotes the Kronecker product, and $\mathbf{H} = [\mathbf{h}(\mathbf{p}_1)^T, \ldots, \mathbf{h}(\mathbf{p}_{n_s})^T]^T$. For the convenience of maximum likelihood calculation, we take the natural logarithm of both sides of Eq. (20), i.e.,

$$\ln[p(\mathbf{Y}|\mathbf{B}, \boldsymbol{\Sigma}, \boldsymbol{\kappa})] = -\frac{n_q n_s}{2}\ln(2\pi) - \frac{n_s}{2}\ln(\det \boldsymbol{\Sigma}) - \frac{n_q}{2}\ln(\det \mathbf{R}) - \frac{1}{2}\mathrm{vec}(\mathbf{Y} - \mathbf{HB})^T (\boldsymbol{\Sigma} \otimes \mathbf{R})^{-1} \mathrm{vec}(\mathbf{Y} - \mathbf{HB}) \tag{21}$$

The maximum likelihood estimation of $\mathbf{B}$ can be derived by setting the derivative of Eq. (21) with respect to $\mathbf{B}$ to be zero [16]. We obtain

$$\tilde{\mathbf{B}} = [\mathbf{H}^T \mathbf{R}(\boldsymbol{\kappa})^{-1} \mathbf{H}]^{-1} \mathbf{H}^T \mathbf{R}(\boldsymbol{\kappa})^{-1} \mathbf{Y} \tag{22}$$

The maximum likelihood estimation of $\boldsymbol{\Sigma}$ is given as [35]

$$\tilde{\boldsymbol{\Sigma}} = \frac{1}{n_s}(\mathbf{Y} - \mathbf{H}\tilde{\mathbf{B}})^T \mathbf{R}(\boldsymbol{\kappa})^{-1} (\mathbf{Y} - \mathbf{H}\tilde{\mathbf{B}}) \tag{23}$$

Since $\mathbf{R}(\boldsymbol{\kappa})$ is only dependent upon the hyperparameters $\boldsymbol{\kappa}$, $\tilde{\mathbf{B}}$, and $\tilde{\boldsymbol{\Sigma}}$ also become functions of $\boldsymbol{\kappa}$. Therefore the maximum likelihood value can be numerically solved from Eq. (21) with respect to parameters $\boldsymbol{\kappa}$. After we obtain the optimal $\tilde{\boldsymbol{\kappa}}$, $\tilde{\mathbf{B}}$, and $\tilde{\boldsymbol{\Sigma}}$ can be obtained sequentially by substituting $\tilde{\boldsymbol{\kappa}}$ into Eqs. (22) and (23).

After the hyperparameters $\tilde{\phi} = \{\tilde{\mathbf{B}}, \tilde{\boldsymbol{\Sigma}}, \tilde{\boldsymbol{\kappa}}\}$ are determined, the MRGP metamodel is established. Under a new input $\mathbf{p}$, i.e., new uncertain parameter set, the posterior of the output is Gaussian with mean and covariance specified as

$$\mathbf{e}[\mathbf{y}(\mathbf{p})] = \mathrm{E}[\mathbf{y}(\mathbf{p})|\mathbf{Y}, \tilde{\phi}] = \mathbf{h}(\mathbf{p})\tilde{\mathbf{B}} + \mathbf{r}(\mathbf{p})\mathbf{R}(\tilde{\boldsymbol{\kappa}})^{-1}(\mathbf{Y} - \mathbf{H}\tilde{\mathbf{B}}) \tag{24}$$

$$\boldsymbol{\sigma}[\mathbf{y}(\mathbf{p})] = \mathrm{Cov}[\mathbf{y}(\mathbf{p})|\mathbf{Y}, \tilde{\phi}] = \tilde{\boldsymbol{\Sigma}}[1 - \mathbf{r}(\mathbf{p})\mathbf{R}(\tilde{\boldsymbol{\kappa}})^{-1}\mathbf{r}(\mathbf{p})] \tag{25}$$

where $\mathrm{E}[\cdot]$ is the expectation operator and $\mathbf{r}(\mathbf{p})$ is an $n_s \times 1$ column vector, the ith element of which is $R(\mathbf{p}, \mathbf{p}_i)$. The output then can be treated as variables satisfying the multivariable Gaussian distribution with the mean and covariance given above. The probability density can be expressed as

$$p(\mathbf{y}|\mathbf{p}, \mathbf{Y}, \mathbf{P}, \tilde{\phi}) = \frac{1}{(2\pi)^{n_q/2}|\boldsymbol{\sigma}|^{1/2}} \exp\left(-\frac{1}{2}(\mathbf{y} - \mathbf{e})\boldsymbol{\sigma}^{-1}(\mathbf{y} - \mathbf{e})^T\right) \tag{26}$$

The mean value in Eq. (24) gives the best prediction of FRF parameters (i.e., the parameters involved in the rational fraction expression of FRF) under the given uncertainty $\mathbf{p}$ as it has the highest probability density. The predicted FRFs can be retrieved by inserting these FRF parameters into Eq. (8).

It is worth noting that the number of output variables in this metamodel for FRF prediction is generally greater than those involved in previous studies using MRGP [16,17]. As such, the actual implementation should pay attention to numerical stability, which is summarized as follows:

(1) In uncertainty analysis of FRFs, we often have $n_q > n_u$, i.e., the number of output variables employed to parametrize the FRF is greater than that of the input variables (i.e., the uncertainty parameters). Under small uncertainties, the difference in each set of output variables is approximately proportional to the difference of uncertainty parameters. If n_q is significantly larger than n_u, the condition number of $\boldsymbol{\Sigma}$ will become very large as some outputs may become linearly dependent. Therefore, in actual implementation, n_q will need to be carefully selected.

(2) The determinants of $\boldsymbol{\Sigma}$ and $\mathbf{R}$ need to be calculated in Eq. (21). In certain cases, these two matrices are close to being singular. We can carry out the LU decomposition of these matrices and then compute the determinants through taking the logarithm, e.g.,

$$\boldsymbol{\Sigma} = \mathbf{LU} \tag{27a}$$

$$\ln[\det(\boldsymbol{\Sigma})] = \sum_{i=1}^{n_q} \ln(U_{ii}) \tag{27b}$$

where $\mathbf{L}$ and $\mathbf{U}$ are lower and upper triangular matrices, respectively, and U_{ii} is the ith diagonal element of $\mathbf{U}$.

(3) The parameters involved in FRF parametrization (Eq. (1)) may have significant differences in their magnitudes. A normalization procedure will help improve the computational performance. Consider real(μ_1) in $\boldsymbol{\alpha}_1$ as an example. A total of n_s real(μ_1) values are obtained from n_s FRF samples. We define

$$\widetilde{\text{real}(\mu_1)}_i = [\text{real}(\mu_1)_i - \overline{\text{real}(\mu_1)}]/\sigma_{\text{real}(\mu_1)}, \quad i = 1, \ldots, n_s \tag{28}$$

where $\overline{\text{real}(\mu_1)}$ and $\sigma_{\text{real}(\mu_1)}$ denote the mean and standard deviation of real(μ_1). $\widetilde{\text{real}(\mu_1)}$ denotes the modified value after the normalization, and it has a mean of 0 and a standard deviation of 1. It is also necessary to perform a similar procedure at the input site, i.e., to transform each uncertainty parameter into the normalized range of [0, 1].

(4) Pre-scanning of $\boldsymbol{\kappa}$ is required to determine the initial value of numerical maximizing problems which can increase the convergence rate. A convenient way to do the scan is setting each element in $\boldsymbol{\kappa}$ to be the same and using simple loop to enumerate each possible value in a logarithmic scale (base 10). Figure 1 shows an example of pre-scanning, where the x-axis is the log base 10 of $\boldsymbol{\kappa}$ and the y-axis is the nature logarithm of the likelihood. The $\boldsymbol{\kappa}$ value achieving the best likelihood value can be used as the initial value.

3.2 Uncertainty Identification of Frequency Response Function Using Bayesian Inference. The MRGP-based formulation can facilitate the forward analysis of uncertainty effects in a frequency response function after it is parametrized through the vector fitting method. Owing to the accuracy of the metamodel, we can update it through uncertainty identification, i.e., quantifying the uncertainty parameters, when new sampled FRFs become available. This can now be realized by incorporating Bayesian inference into the MRGP modeling.

Given samples of observed response $\mathbf{Y}$ at n_s uncertainty input $\mathbf{P}$, the MRGP model is established with hyperparameters $\tilde{\phi} = \{\tilde{\mathbf{B}}, \tilde{\boldsymbol{\Sigma}}, \tilde{\boldsymbol{\omega}}\}$ as outlined in Sec. 3.1. This metamodel can provide the probability of an arbitrary output vector $\mathbf{y}$ under the given samples and an arbitrary input $\mathbf{p}$ as $p(\mathbf{y}|\mathbf{p}, \mathbf{Y}, \mathbf{P}, \tilde{\phi})$ shown in Eq. (26). We assume that a new given family of FRFs with unknown uncertainty parameters are parameterized into vector $\hat{\mathbf{y}}$ by means of vector vetting. We can estimate the posterior of uncertainty parameters $\mathbf{p}$ according to Bayesian inference

$$p(\mathbf{p}|\hat{\mathbf{y}}, \mathbf{Y}, \mathbf{P}, \tilde{\phi}) = \frac{p(\hat{\mathbf{y}}|\mathbf{p}, \mathbf{Y}, \mathbf{P}, \tilde{\phi})p(\mathbf{p})}{p(\hat{\mathbf{y}}|\tilde{\phi})} \tag{29}$$

where the conditional probability $p(\hat{\mathbf{y}}|\mathbf{p}, \mathbf{Y}, \mathbf{P}, \tilde{\phi})$ can be calculated by using Eq. (26) from the MRGP metamodel, and $p(\mathbf{p})$ is the prior of the uncertainty parameters. The denominator can be determined as

$$p(\hat{\mathbf{y}}|\tilde{\phi}) = \oint p(\hat{\mathbf{y}}|\mathbf{p}, \mathbf{Y}, \mathbf{P}, \tilde{\phi})p(\mathbf{p})\mathrm{d}p_1\mathrm{d}p_2 \ldots \mathrm{d}p_{n_u} \tag{30}$$

where $\mathrm{d}p_i$ $(i = 1, \ldots, n_u)$ denotes the differential of each component in the input vector. A common practice is to take $p(\hat{\mathbf{y}}|\tilde{\phi})$ as a normalization constant.

The posterior actually gives the specific probabilistic distribution of uncertainty parameters for the new given FRFs under the condition of samples and prior knowledge. $\hat{\mathbf{p}}$ that maximizes $p(\mathbf{p}|\hat{\mathbf{y}}, \mathbf{Y}, \mathbf{P}, \tilde{\phi})$ represents the uncertainty parameters that have the highest possibility to generate the FRF parameters. In other words, this $\hat{\mathbf{p}}$ can be regarded as the quantified or identified uncertainty parameters for the system that generates the new given FRF. Maximizing the likelihood function Eq. (29) with respect to $\mathbf{p}$ yields the quantification of uncertainty parameters. As $p(\hat{\mathbf{y}}|\mathbf{p})$ is not computed, we only need to apply the maximization to $p(\hat{\mathbf{y}}|\mathbf{p}, \mathbf{Y}, \mathbf{P}, \tilde{\phi})p(\mathbf{p})$. Typically, one takes the natural logarithm of this probability density to facilitate computation [34]

$$\begin{aligned} p_{\ln} = \ln[p(\hat{\mathbf{y}}|\mathbf{p}, \mathbf{Y}, \mathbf{P}, \tilde{\phi})p(\mathbf{p})] = -\frac{n_q}{2}\ln(2\pi) - \frac{1}{2}\ln(|\boldsymbol{\sigma}|) \\ -\frac{1}{2}(\hat{\mathbf{y}} - \mathbf{e})\boldsymbol{\sigma}^{-1}(\hat{\mathbf{y}} - \mathbf{e})^T + \ln[p(\mathbf{p})] \end{aligned} \tag{31}$$

A number of studies utilize the gradient methods or local perturbation, e.g., Markov Chain Monte Carlo, to carry out optimization. It is, however, possible for the solution to be trapped at a local maximum, which will be illustrated in the case studies in Sec. 4. Many recent investigations employ heuristic optimization approaches [36] such as genetic algorithm [37] or particle swarm optimization [38,39] to find the global optimum. In this research, we employ the particle swarm algorithm for all the following identification analysis.

Figure 2 shows the flowchart that explains how to build an MRGP model from FRFs and how the MRGP model is used for FRF prediction and parameter identification. It also illustrates how the concepts, such as vector fitting, Bayesian inference, are involved in the entire analysis procedure.

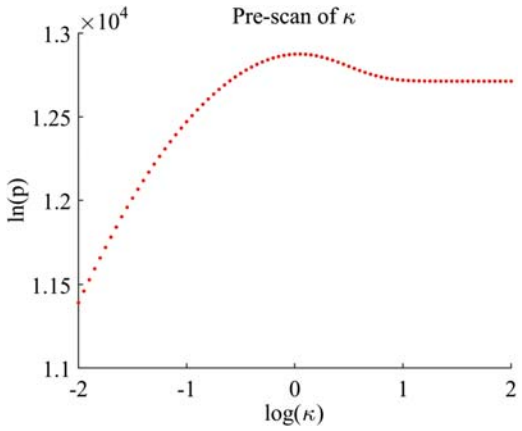

Fig. 1 Pre-scanning example

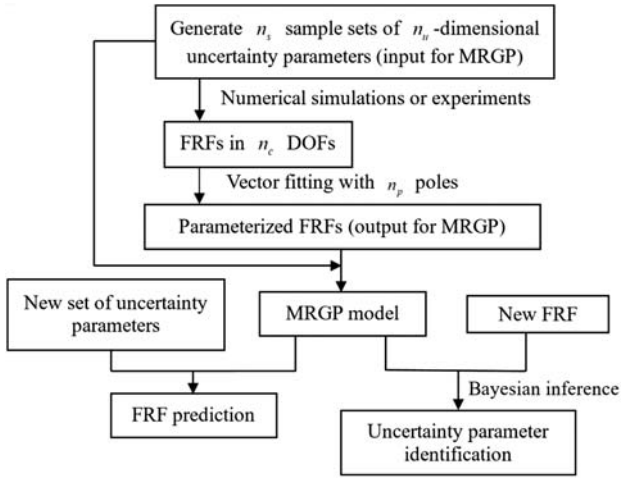

Fig. 2 Flowchart of MRGP establishment and application

4 Case Illustration and Discussion

In this section, two carefully designed cases are presented to illustrate the implementation of the approach developed and to demonstrate the effectiveness. A discrete, spring-mass-damper model is employed to verify the forward and inverse analysis of uncertainty effects, where insights to the numerical implementation are provided. A beam finite element model is then adopted to show the potential application of this analysis in structural damage detection.

4.1 MRGP Based Metamodeling and Uncertainty Quantification Applied to Discrete System

4.1.1 Case Definition. In this first illustration, we analyze a 10DOF structure as shown in Fig. 3. The nominal structure without uncertainties has stiffness $k=4\pi^2$ and mass $m_0=1$. The masses are numbered from 1 to 10 sequentially from left to right. The mass and stiffness matrices of the nominal structure, denoted as $\mathbf{M}_0$ and $\mathbf{K}_0$, can be easily obtained. We assume proportional damping, i.e.,

$$\mathbf{C}_0 = 0.01\mathbf{M}_0 + 0.0001\mathbf{K}_0$$

We further assume that in all the subsequent analyses of this structure, uncertainties occur as the changes of masses, i.e.,

$$m_i = m_0 + \Delta m_i, \quad i = 1, \ldots, 10$$

Therefore, the actual mass matrix becomes $\mathbf{M} = \mathbf{M}_0 + \Delta\mathbf{M}$. A unit excitation is applied to the first mass and we can acquire the FRFs of any mass directly. These FRFs can be parameterized by the vector fitting method for building the MRGP metamodel.

4.1.2 Forward Analysis of Uncertainty Effects. We assume n_u masses, numbered from $(11-n_u)$ to 10, respectively, are subjected to uncertainties. Cases with different n_u are to be analyzed. At input site, the uncertainty parameter Δm_i is assumed to be uniformly distributed within the range $[-0.05, 0.05]$, and Latin hypercube sampling [40] is adopted to acquire the sampled uncertainties. The frequency range of interest is [0.7, 1.4], and the frequency resolution of FRF used is 0.001. We focus on the FRF of mass 10, i.e., $n_c=1$. As three natural frequencies can be found within the interested frequency range for the nominal system without uncertainty, the number of poles in the vector fitting method is chosen to be $n_p = 2\times 3+4=10$. Therefore, the dimension at the output site is $n_q = n_p\times(n_c+1)=20$.

We acquire n_s sampled FRF responses, which in this simulation case are obtained by direct calculation from the equation of motion, as the training data. Following the procedures outlined in Secs. 2.2 and 3.1, we can obtain the MRGP metamodel. The sample size of the training data used in constructing the MRGP metamodel, n_s, varies as n_u varies because larger n_u generally requires larger n_s. In Table 1, we list the performance of the metamodel obtained under different n_u. We compare the FRF results predicted by the MRGP metamodel with those obtained from direct computation from the equation of motion. The relative error of directly calculated FRF $T(\omega)$ and the predicted FRF $\tilde{T}(\omega)$ from the MRGP metamodel at each frequency point is defined as

$$\Delta T(\omega_i) = \frac{||T(\omega_i)| - |\tilde{T}(\omega_i)||}{|T(\omega_i)|}, \quad i = 1, \ldots, n_\omega$$

Table 1 FRF forward analysis case comparison

Case #	n_u	n_s	Average of max error $\Delta\bar{T}$ (%)	Average of mean error max (ΔT) (%)
1	4	50	0.081	0.890
2	5	50	0.095	1.148
3	6	50	0.263	4.290
4	7	50	0.464	8.290
5	8	50	0.650	12.653
6	9	50	0.720	13.664
7	10	50	0.819	16.083
8	7	60	0.293	4.821
9	7	70	0.151	2.215
10	7	80	0.110	1.400
11	7	90	0.087	1.023
12	7	100	0.075	0.812
13	8	100	0.108	1.404
14	9	100	0.200	3.344
15	10	100	0.326	5.416

where n_ω is the number of frequency points. We further define the mean and maximum relative errors of an FRF as

$$\Delta\bar{T} = \frac{1}{n_\omega}\sum_{i=1}^{n_\omega}\Delta T(\omega_i), \qquad \max(\Delta T) = \max[\Delta T(\omega_i)]$$

For each case listed in Table 1, the statistical averages of $\Delta\bar{T}$ and $\max(\Delta T)$ are calculated based on 1000 samples of uncertainty parameters. As shown in the table, the mean errors in all cases are generally small. From case 1 to case 7 with the training data size $n_s=50$, we can observe that the maximum error increases as the number of uncertainty parameters increases, since the size of the training data remains unchanged. Case 4 along with case 8 to case 12 indicate that as we increase the size of the training data while maintaining the number of uncertain parameters, the relative errors are significantly reduced. Case 13 to case 15 show the same trend that relative errors are reduced as the size of the training data is increased from 50 to 100. The size of training data is an important parameter, and a larger size usually leads to a better MRGP prediction. While it is impossible to decide *a priori* the necessary size of training data, in general it can be determined through convergence analysis whereas the size (i.e., the number of training datasets) increases.

Figure 4 shows a representative example of FRF comparison with $n_u=7$ and $n_s=100$. The values of Δm_i $(i=4,\ldots,10)$ equal to $[0.1715, 4.7190, -2.7771, -2.9472, -3.0778, -1.3686, -0.1307]\times 10^{-2}$, respectively, which are randomly generated. The amplitude and phase under this specific set uncertain parameters predicted from the MRGP metamodel match well with the results from direct real model calculation. Within the entire frequency range of interest, the relative error in amplitude is smaller than 1% and the absolute error in phase is virtually negligible. These results indicate that the proposed forward analysis approach using MRGP-based metamodel can be a viable tool to evaluate uncertainty effects.

4.1.3 Inverse Analysis: Uncertainty Parameter Quantification. In this subsection, we illustrate the quantification of uncertainty parameters using MRGP metamodeling incorporated with Bayesian inference. In this type of analyses, in practical situations, we are usually given a set of FRF results obtained experimentally. Here, in this case study, we use simulated data of FRF results as input.

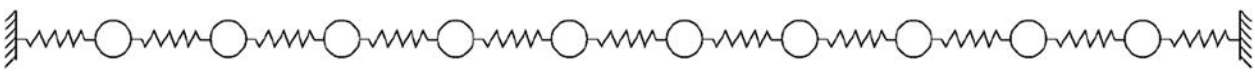

Fig. 3 Discrete structure configuration

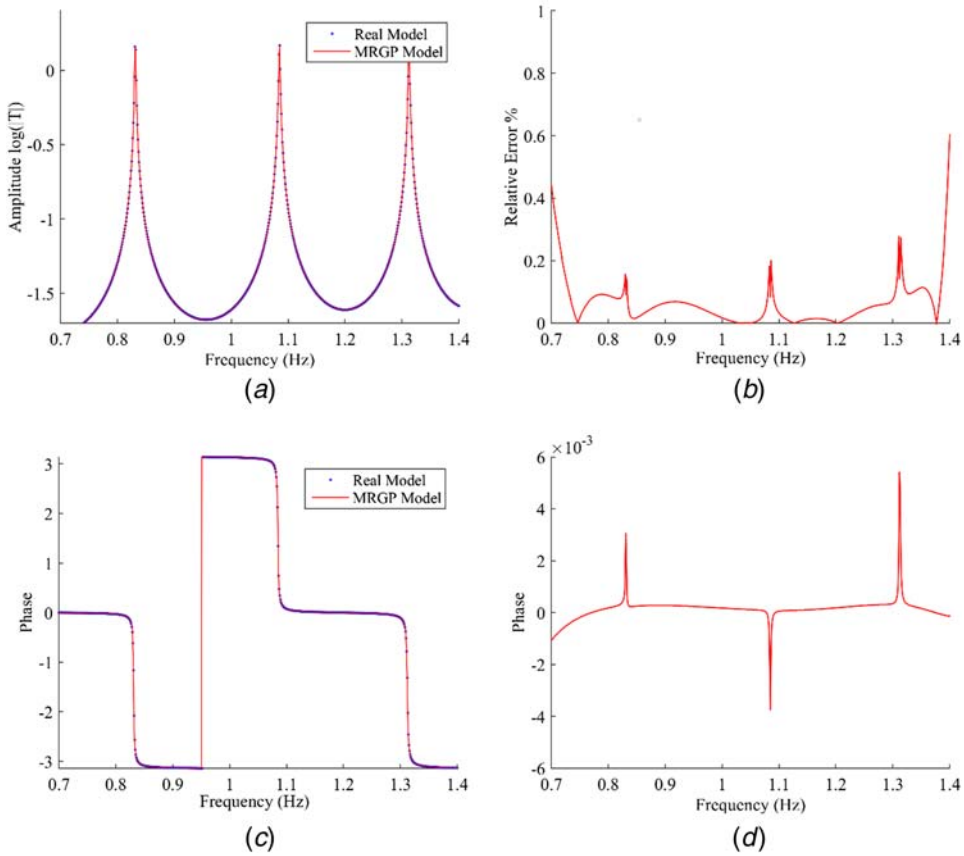

Fig. 4 (*a*) Example of FRF amplitude, (*b*) relative error in amplitude, (*c*) example of FRF in phase, and (*d*) absolute error in phase

To assess the performance of the algorithm, we let the masses (numbered from $(11-n_u)$ to 10 in each case) be subjected to uncertainties, where n_u is the number of uncertainty parameters. Then, n_s sampled FRF results from n_c observation locations are used to generate the corresponding MRGP metamodel. The datasets involved are generated directly from the system equation with n_u uncertainty parameters sampled within the range $[-0.05, 0.05]$. The observation locations are specific masses whose FRFs are observed for MRGP metamodel establishment. Without loss of generality, the prior of the uncertainty parameter $p(\mathbf{p})$ for Bayesian inference in Eq. (29) is chosen to be the same uniform distribution $U[-0.05, 0.05]$. Finally, for any new given FRF, the algorithm is capable of quantifying the uncertainty parameters that are most likely to generate this FRF based on Bayesian inference and the procedure of maximizing likelihood. Particle swarm optimization is employed and, in this section for uncertainty parameters normalized to range [0, 1], the maximum velocity in one direction, the cognitive constant, and the social constant for this algorithm are set to be 0.01, 0.1, and 0.1, respectively. A number of scenarios are analyzed to assess different parametric choices (n_s, n_c, and frequency sampling interval of FRF) and different locations of observation (i.e., different mass elements). Table 2 lists the parameters of cases analyzed.

In case 1, the structure has two uncertain mass parameters, which makes it possible to show the likelihood value in a 3-dimensional contour. This case helps to illustrate localized maximum phenomenon mentioned in Sec. 3.2. Figure 5 shows an example of the adjusted equivalent likelihood value generated from Eq. (29) versus two parameters. Several local maxima are found, indicating that gradient-based methods could not yield a satisfying result. This phenomenon is more critical if the number of uncertainty parameters to be quantified is large. Therefore, self-adaptation optimization, particle swarm optimization [38], is adopted hereafter.

In case 2 to case 7, the number of uncertainty parameters remains to be 10, which means all masses are subjected to uncertainty. Different MRGP metamodels are built for each case according to the parameters listed in Table 2, and they will be used for quantification in the subsequent investigation. Without loss of generality, we choose randomly the set of 10 uncertainty parameters $[-3.102, -3.820, 4.193, 3.879, -0.764, -2.246, 1.310, 3.093, -2.485, 3.429]\times 10^{-2}$ to build a system with uncertainty and calculate its corresponding FRFs at assigned output locations (different mass locations). We then take these FRFs as input to quantify the uncertainty parameters. These FRFs are parameterized by using the vector fitting method, and the results are employed in uncertainty quantification based on Bayesian inference and different MRGP metamodel in each case. The results are listed in Table 3.

Obviously, case 2 fails to deliver a good result as it has a large maximum error. This indicates that only one output location is insufficient to conduct quantification for a large number of uncertainty parameters. Case 3 and case 5 both successfully complete

Table 2 Case parameters for uncertainty parameter quantification

Case	n_u	n_s	n_c	Mass number	Frequency sampling interval
1	2	40	1	10	0.001
2	10	100	1	5	0.001
3	10	100	2	3,7	0.001
4	10	50	2	3,7	0.001
5	10	100	3	3,5,7	0.001
6	10	100	2	5,7	0.001
7	10	100	2	3,7	0.01

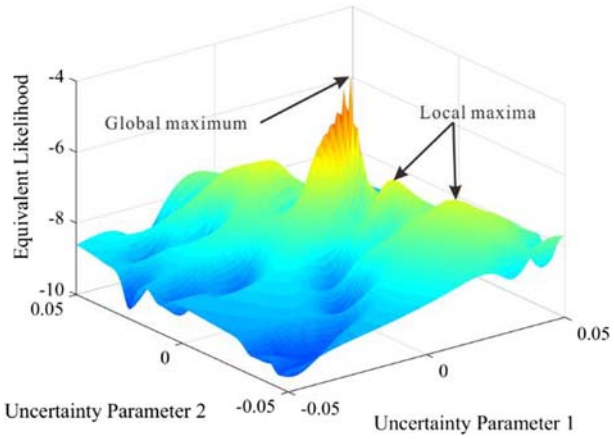

Fig. 5 Local maxima illustration

the quantification with good accuracy based on FRFs at multiple output locations. Figure 6(*a*) shows FRF amplitude results of case 3, in the FRF derived from the given original uncertainty parameters (i.e., actual value) and that derived from the quantified uncertainty parameters are compared. The two results match with each other well, and the relative error shown in Fig. 6(*b*) is very small. The number of observation output locations should be increased if the number of uncertainty parameters to be quantified increases.

Cases 3 and 4 have a different number of samples n_s, whereas other parameters remain the same. Case 3 has a smaller error, indicating that the increase of sample size used in MRGP metamodel increases the accuracy of quantification. Cases 3 and 6 both have two output locations but the actual output locations are different. Apparently, case 6 has poor performance as it has a larger maximum error. The reason is that the output locations in case 6 only focus on the right-hand side of the system. It indicates that the choice of output location should be carefully considered, and the desired output locations should have their FRFs more sensitive

Table 3 Quantification results for different cases

Δm_i/1E-2	1	2	3	4	5	6	7	8	9	10	Max error
Actual value	−3.102	−3.820	4.193	3.879	−0.764	−2.246	1.310	3.093	−2.485	3.429	—
Case 2	−4.081	−3.277	4.201	3.317	0.120	−3.305	1.733	2.968	−2.953	4.598	1.169
Case 3	−3.159	−3.787	4.238	3.850	−0.740	−2.198	1.308	3.070	−2.475	3.463	0.057
Case 4	−3.201	−3.834	4.330	3.828	−0.952	−2.231	1.434	2.910	−2.562	3.651	0.222
Case 5	−3.015	−3.872	4.154	3.893	−0.796	−2.249	1.315	3.171	−2.457	3.382	0.087
Case 6	−2.521	−3.120	4.752	3.122	−2.032	−2.272	1.425	3.172	−2.382	3.406	1.268
Case 7	−3.215	−3.950	3.748	3.327	−0.845	−1.788	2.062	3.153	−2.498	3.368	0.752

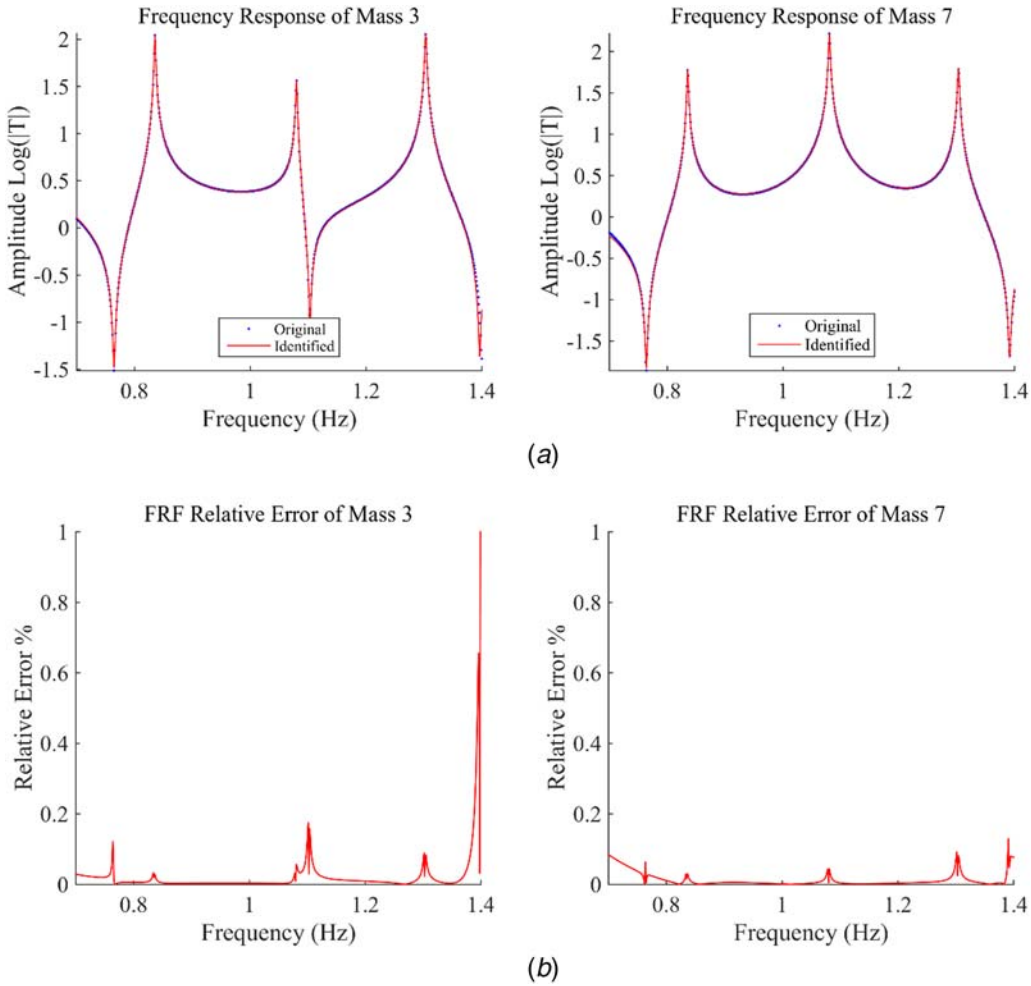

Fig. 6 (*a*) FRF amplitude results of case 3 and (*b*) relative error in amplitude of case 3

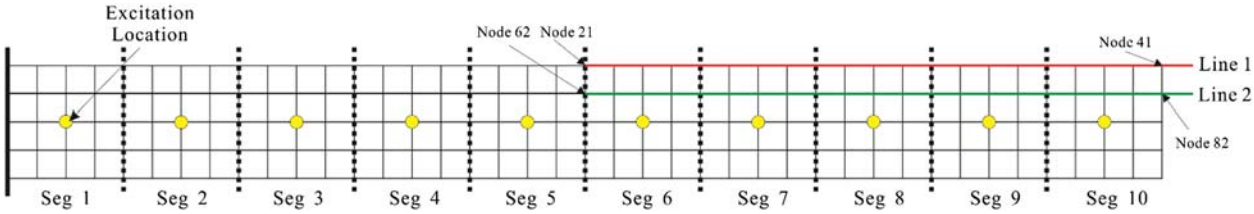

Fig. 7 Beam structure. The finite element model is divided into 10 segments. For each segment, change of mass (due to either uncertainty or damage occurrence) is concentrated at the center node.

to the variation of uncertainty parameters. Consideration must be given to the spatial distribution of uncertainty parameters. In our system, case 3 gathers information from both the left-hand side and the right-hand side, which indeed yields a better result. Case 3 and case 7 have different frequency sampling intervals for FRFs, while other parameters remain the same. A larger frequency sampling interval in case 7 deteriorates the fidelity of sampled FRFs. As a result, case 7 has larger error than case 3.

The abovementioned cases demonstrate the effectiveness of combining MEGP metamodel with Bayesian inference to quantify the uncertainty parameters and illustrate the influences of various parameters, e.g., the number of samples, the number and the location of the FRF observation, as well as the frequency sampling interval of FRFs.

4.2 MRGP Metamodel of Beam Structure Frequency Response Function Employed for Damage Detection. In this section, we present another illustration based on a cantilever beam, which is essentially a continuous structure. Since damage effect causes a change of structural properties, whereas uncertainties are generally present, we further extend the analysis to demonstrate the capability of the proposed method in structural damage detection through parametric identification.

Table 4 FRF parameters from direct calculation and MRGP model prediction

Poles	FRF parameters	Direct calculation	MRGP model prediction
1	μ_1	$-0.751 \pm 1.264\text{E}2i$	$-1.349 \pm 1.337\text{E}2i$
	γ_{11}	$-1.971\text{E}{-7} \mp 1.916\text{E}{-4}i$	$-3.904\text{E}{-7} \mp 1.793\text{E}{-4}i$
	γ_{12}	$-3.978\text{E}{-7} \mp 3.231\text{E}{-4}i$	$-6.448\text{E}{-7} \mp 3.025\text{E}{-4}i$
2	μ_2	$-3.320\text{E}{-2} \pm 6.636\text{E}2i$	$-3.320\text{E}{-2} \pm 6.636\text{E}2i$
	γ_{21}	$-1.190\text{E}{-10} \mp 1.126\text{E}{-4}i$	$-2.139\text{E}{-10} \mp 1.126\text{E}{-4}i$
	γ_{22}	$7.847\text{E}{-11} \pm 3.550\text{E}{-4}i$	$5.307\text{E}{-10} \pm 3.550\text{E}{-4}i$
3	μ_3	$-9.280\text{E}{-2} \pm 1.856\text{E}3i$	$-9.280\text{E}{-2} \pm 1.856\text{E}3i$
	γ_{31}	$1.860\text{E}{-8} \pm 2.034\text{E}{-4}i$	$1.347\text{E}{-8} \pm 2.034\text{E}{-4}i$
	γ_{32}	$-2.845\text{E}{-8} \mp 3.112\text{E}{-4}i$	$-2.051\text{E}{-8} \mp 3.112\text{E}{-4}i$
4	μ_4	$-2.732\text{E}2 \pm 3.493\text{E}3i$	$-1.914\text{E}2 \pm 3.493\text{E}3i$
	γ_{41}	$1.440\text{E}{-6} \mp 9.750\text{E}{-5}i$	$1.948\text{E}{-7} \mp 9.666\text{E}{-5}i$
	γ_{42}	$-5.262\text{E}{-6} \pm 1.815\text{E}{-4}i$	$-5.032\text{E}{-6} \pm 1.826\text{E}{-4}i$

Similar to the lumped mass-spring system analyzed in Sec. 4.1, uncertainty, possibly due to damage, is introduced as the variation of mass in the model. We assume, without loss of generality, that the structural damage causes property change of the model which is quantified as local mass change [41,42]. In order to yield a realistic and computationally tractable analysis, we divide the beam finite element model into 10 segments numbered from 1 (left end) to 10 (right end). We further let the change of mass be concentrated at the center node of each segment (Fig. 7).

We start from developing the MRGP metamodel of the beam structure, where five uncertainty parameters representing potential mass losses due to damage are introduced to the center nodes of segment 6 to segment 10. Each uncertainty parameter is subjected to uniform distribution within the range [−0.001, 0], indicating potential mass loss with the maximum being 0.001 kg (0.16% of the total mass of the beam). An excitation is applied to the center node of segment 1, perpendicular to the beam surface and with constant magnitude 1 N. The FRFs are observed/measured from center nodes of segment 7 and segment 10. The frequency range of FRFs is from 50 to 350 Hz with a sampling interval of 0.1 Hz. The damping coefficient for frequency response analysis in

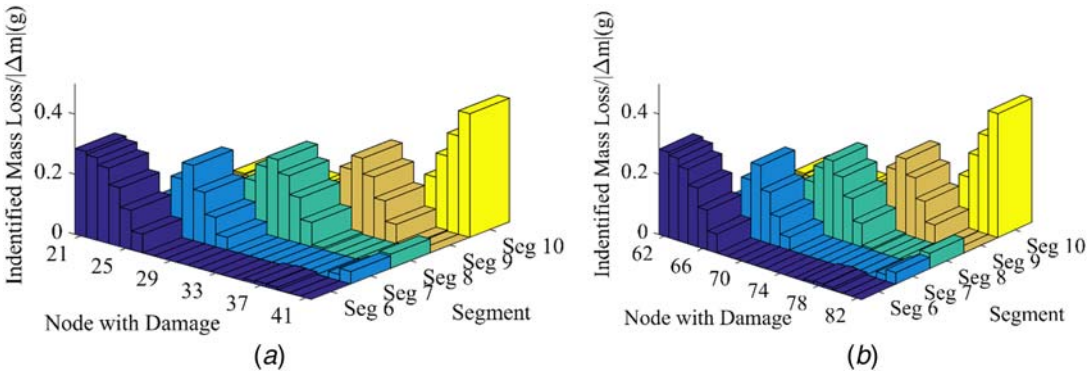

Fig. 8 (*a*) Identification results for nodes with damage in line 1 and (*b*) identification results for nodes with damage in line 2

Patran/Nastran is set to be 1×10^{-4} [43]. Within this range, two resonant frequencies exist, and therefore $n_p = 2 \times 2 + 4 = 8$ poles are chosen for vector fitting. Hundred samples of uncertainty parameters are generated through Latin hypercube sampling. The corresponding FRFs are then acquired by using the Patran/Nastran solver and subsequently parameterized through the vector fitting method. An MRGP metamodel is then established based on the approach outlined in Sec. 3.1.

We first examine the validity of the MRGP metamodel. We compare the vector-fitted FRF results from both direct calculations using finite element analysis and from prediction using MRGP metamodel. The uncertainty parameters as inputs are randomly chosen as $[-0.418, -0.459, -0.130, -0.735, -0.682] \times 10^{-3}$ kg. The results of parameterized FRFs from two approaches are listed in Table 4. It can be observed that the MRGP metamodel can predict these parameters with very good accuracy. With an Intel i7-7820HQ CPU, the computational times for direct analysis using finite element and using MRGP metamodel are, respectively, 11.21 s and 1.38×10^{-4} s. Apparently, the MRGP metamodel would entertain significant advantage in computational efficiency when dealing with large-scale problems. It is worth noting that essentially the establishment of MRGP metamodel only requires FRF information. Therefore, while simulation datasets are used in this paper, the proposed framework can directly employ experimental data (without involving the numerical model) in practice.

We then utilize the MRGP metamodel obtained to perform system identification and damage detection. We assume single damage occurrence [41,42] quantified as mass loss at a single node. In Fig. 7, line 1 and line 2 contain nodes 21–41 and nodes 62–82. The mass loss is applied to each individual node among these nodes one by one, and altogether we then have 42 cases. For each case, a 2.5×10^{-4} kg mass loss applied. The FRF of each case is calculated by Nastran and then parameterized by the vector fitting method for identification purpose. As the MRGP metamodel is built based on mass variations in center nodes of specific segments, the identification results here are the mass losses at the center nodes. As a segment is small, the mass loss at the center node can also be regarded to represent the mass loss of this segment during identification. Figures 8(*a*) and 8(*b*) show the results corresponding to nodes with mass losses in line 1 and line 2. In each identification case, the segment with maximal quantified uncertainty parameter value is in accordance with the actual damage location (i.e., the segment to which the damage node belongs). Also, the quantified mass loss value in that segment is very close to the actual mass loss value 2.5×10^{-4} kg. In some cases (e.g., node 25 and node 66), both two neighboring segments show conspicuous values identified, which is in accordance with the fact that damage is located on the boundary of these two segments. These two figures look similar, indicating that the system is not sensitive to mass loss shifted in the width direction. This is because the width of beam is small. Nevertheless, the identified parameters successfully mark the damage segment location. MRGP can identify the damage segment even if the mass loss is not located at the center of the segment or along the center line of the beam width, revealing the good robustness of MRGP.

5 Concluding Remarks

In this research, the uncertainty analysis and quantification of vibration systems utilizing their FRFs through statistical metamodeling are presented. The metamodel development is built upon the MRGP approach which takes advantage of the inherent correlation of FRF values at different frequency points. To facilitate the implementation, a rational approximation of FRF by means of vector fitting is incorporated. Based on sampling data, a well-built MRGP model is capable of predicting FRF values when new uncertainty parameters are given. Meanwhile, to fully utilize the MRGP metamodeling, we further integrate Bayesian inference to realize model updating and uncertainty quantification as new FRFs are acquired. Two case studies, a lumped parameter mass-spring structure and a beam structure discretized by finite element modeling, are analyzed to verify the proposed framework. The results indicate that the MRGP metamodel can predict and quantify uncertainty effects to FRF efficiently and accurately. The MRGP metamodel with the assistance of Bayesian inference can effectively identify parametric variation in the underlying structure, which can be used to realize damage detection and identification.

Funding Data

- The National Natural Science Foundation of China under Grant No. 11572089, by China Scholarship Foundation under Grant No. 201606100140, and by the National Science Foundation under Grant IIS—1741171.

References

[1] Brincker, R., Zhang, L., and Andersen, P., 2000, "Modal Identification From Ambient Responses Using Frequency Domain Decomposition," IMAC 18: Proceedings of the International Modal Analysis Conference (IMAC), San Antonio, TX, Feb. 7–10, pp. 625–630.

[2] Shu, L., Wang, M. Y., Fang, Z., Ma, Z., and Wei, P., 2011, "Level set Based Structural Topology Optimization for Minimizing Frequency Response," J. Sound Vib., **330**(24), pp. 5820–5834.

[3] Bandara, R. P., Chan, T. H. T., and Thambiratnam, D. P., 2014, "Frequency Response Function Based Damage Identification Using Principal Component Analysis and Pattern Recognition Technique," Eng. Struct., **66**(4), pp. 116–128.

[4] Limongelli, M. P., 2010, "Frequency Response Function Interpolation for Damage Detection Under Changing Environment," Mech. Syst. Signal Process., **24**(8), pp. 2898–2913.

[5] Kim, C. J., Oh, J. S., and Park, C. H., 2014, "Modelling Vibration Transmission in the Mechanical and Control System of a Precision Machine," CIRP Ann. Manuf. Technol., **63**(1), pp. 349–352.

[6] Hu, J., Sun, L., Yuan, X., Wang, S., and Chi, Y., 2017, "Modeling of Type 3 Wind Turbine With df/dt Inertia Control for System Frequency Response Study," IEEE Trans. Power Syst. **32**(4), pp. 2799–2809.

[7] Xia, Z., and Tang, J., 2013, "Characterization of Dynamic Response of Structures With Uncertainty by Using Gaussian Processes," ASME J. Vib. Acoust., **135**(5), p. 051006.

[8] Muscolino, G., Santoro, R., and Sofi, A., 2014, "Explicit Frequency Response Functions of Discretized Structures With Uncertain Parameters," Comput. Struct., **133**, pp. 64–78.

[9] Hinke, L., Dohnal, F., Mace, B. R., Waters, T. P., and Ferguson, N. S., 2009, "Component Mode Synthesis as a Framework for Uncertainty Analysis," J. Sound Vib., **324**(1–2), pp. 161–178.

[10] Yang, J., Faverjon, B., Peters, H., Margurg, S., and Kessissoglou, N., 2017, "Deterministic and Stochastic Model Order Reduction for Vibration Analyses of Structures With Uncertainties," ASME J. Vib. Acoust., **139**(2), p. 021007.

[11] Rasmussen, C. E., and Williams, C. K. I., 2006, *Gaussian Processes for Machine Learning*, The MIT Press, Cambridge, MA.

[12] DiazDela, F. A., and Adhikari, O. S., 2010, "Structural Dynamic Analysis Using Gaussian Process Emulators," Eng. Comput., **27**(5), pp. 580–605.

[13] Arendt, P. D., Apley, D. W., and Chen, W., 2012, "Quantification of Model Uncertainty: Calibration, Model Discrepancy, and Identifiability," ASME J. Mech. Des., **134**(10), p. 100908.

[14] Fricker, T. E., Oakley, J. E., Sims, N. D., and Worden, K., 2011, "Probabilistic Uncertainty Analysis of an FRF of a Structure Using a Gaussian Process Emulator," Mech. Syst. Signal Process., **25**(8), pp. 2962–2975.

[15] Diazdelao, F. A., Adhikari, S., Flores, E. I. S., and Friswell, M. I., 2013, "Stochastic Structural Dynamic Analysis Using Bayesian Emulators," Comput. Struct., **120**, pp. 24–32.

[16] Arendt, P. D., Chen, W., and Apley, D. W., 2012, "Improving Identifiability in Model Calibration Using Multiple Responses," ASME J. Mech. Des., **134**(10), p. 100909.

[17] Kontar, R., Zhou, S., and Horst, J., 2017, "Estimation and Monitoring of Key Performance Indicators of Manufacturing Systems Using the Multi-Output Gaussian Process," Int. J. Prod. Res., **55**(8), pp. 2304–2319.

[18] Liu, Y., Zhou, K., and Lei, Y., 2015, "Using Bayesian Inference Framework Towards Identifying Gas Species and Concentration From High Temperature Resistive Sensor Array Data," J. Sens. **2015**, pp. 1–10.

[19] Kennedy, M. C., and O'Hagan, A., 2001, "Bayesian Calibration of Computer Models," J. R. Stat. Soc., **63**(3), pp. 425–464.

[20] Eidsvik, J., Finley, A. O., Banerjee, S., and Havard, R., 2012, "Approximate Bayesian Inference for Large Spatial Datasets Using Predictive Process Models," Comput. Stat. Data Anal., **56**(6), pp. 1362–1380.

[21] Williams, C. K. I., and Barber, D., 1998, "Bayesian Classification With Gaussian Processes," IEEE Trans. Pattern Anal. Mach. Intell., **20**(12), pp. 1342–1351.

[22] Filippone, M., and Girolami, M., 2014, "Pseudo-Marginal Bayesian Inference for Gaussian Processes," IEEE Trans. Pattern Anal. Mach. Intell., **36**(11), pp. 2214–2226.

[23] Gustavsen, B., and Semlyen, A., 1999, "Rational Approximation of Frequency Domain Responses by Vector Fitting," IEEE Trans. Power Delivery, **14**(3), pp. 1052–1061.

[24] Zeng, R. X., and Sinsky, J. H., "Modified Rational Function Modeling Technique for High Speed Circuits," IEEE MTT-S: Proceedings of the International Microwave Symposium, San Francisco, CA, Feb., pp. 1951–1954.
[25] Veletsos, A. S., and Ventura, C. E., 1986, "Modal Analysis of Non-Classically Damped Systems," Earthquake Eng. Struct. Dyn., **14**(2), pp. 217–243.
[26] Einar, N. S., 2014, *Structural Dynamics*, Springer, New York.
[27] Meirovitch, L., 1990, *Dynamics and Control of Structures*, John Wiley & Sons, Hoboken, NJ.
[28] Li, E.-P., Liu, E.-X., Li, L.-W., and Leong, M.-S., 2004, "A Coupled Efficient and Systematic Full-Wave Time-Domain Macromodeling and Circuit Simulation Method for Signal Integrity Analysis of High-Speed Interconnects," IEEE Trans. Adv. Packag., **27**(1), pp. 213–223.
[29] Grivet-Talocia, S., and Bandinu, M., 2006, "Improving the Convergence of Vector Fitting for Equivalent Circuit Extraction From Noisy Frequency Responses," IEEE Trans. Electromagn. Compat., **48**(1), pp. 104–120.
[30] Karimifard, P., Gharehpetian, G. B., and Tenbohlen, S., 2007, "Determination of Axial Displacement Extent Based on Transformer Winding Transfer Function Estimation Using Vector-Fitting Method," Int. Trans. Electr. Energy Syst., **18**(4), pp. 423–436.
[31] Grivet-Talocia, S., and Gustavsen, B., 2015, *Passive Macromodeling: Theory and Applications*, John Wiley & Sons, Hoboken, NJ.
[32] Conti, S., and O'Hagan, A., 2009, "Gaussian Process Emulation of Dynamic Computer Codes," Biometrika, **96**(3), pp. 663–676.
[33] Conti, S., and O'Hagan, A., 2010, "Bayesian Emulation of Complex Multi-Output and Dynamic Computer Models," J. Stat. Plan. Infer., **140**(3), pp. 640–651.
[34] Bilionis, I., and Zabaras, N., 2012, "Multi-Output Local Gaussian Process Regression: Applications to Uncertainty Quantification," J. Comput. Phys., **231**(17), pp. 5718–5746.
[35] Johnson, R. A., and Wichern, D. W., 2002, *Applied Multivariate Statistical Analysis*, Prentice Hall, Upper Saddle River, NJ.
[36] Larrañaga, P., Karshenas, H., Bielza, C., and Santana, R., 2013, "A Review on Evolutionary Algorithms in Bayesian Network Learning and Inference Tasks," Inf. Sci., **233**(2), pp. 109–125.
[37] Deb, K., Pratap, A., Agarwal, S., and Meyarivan, T., 2002, "A Fast and Elitist Multiobjective Genetic Algorithm: NSGA-II," IEEE Trans. Evol. Comput., **6**(2), pp. 182–197.
[38] Eberhart, R., and Kennedy, J., 1995, "A New Optimizer Using Particle Swarm Theory," IEEE MHS'95: The 6th International Symposium on Micro Machine and Human Science, Nagoya, Japan, pp. 39–43.
[39] Sahin, F., Yavuz, MÇ, Arnavut, Z., and Uluyol, O., 2007, "Fault Diagnosis for Airplane Engines Using Bayesian Networks and Distributed Particle Swarm Optimization," Parallel Comput., **33**(2), pp. 124–143.
[40] Iman, R. L., 2008, *Latin Hypercube Sampling*, John Wiley & Sons, Hoboken, NJ.
[41] Wang, X., and Tang, J., 2009, "Damage Identification Using Piezoelectric Impedance Approach and Spectral Element Method," J. Intell. Mater. Syst. Struct., **20**(8), pp. 907–921.
[42] Shuai, Q., Zhou, K., Zhou, S., and Tang, J., 2017, "Fault Identification Using Piezoelectric Impedance Measurement and Model-Based Intelligent Inference With Pre-Screening," Smart Mater. Struct., **26**(4), p. 045007.
[43] MSC Software Corporation, 2012, *MSC Nastran Quick Reference Guide*, MSC Software Corporation, Newport Beach, CA.